Geochemistry Geophysics Geosystems G3
AN ELECTRONIC JOURNAL OF THE EARTH SCIENCES
Published by AGU and the Geochemical Society

Article
Volume 6, Number 10
21 October 2005
Q10005, doi:10.1029/2005GC000935
ISSN: 1525-2027

Triggering of tsunamigenic aftershocks from large strike-slip earthquakes: Analysis of the November 2000 New Ireland earthquake sequence

Eric L. Geist and Tom Parsons
U.S. Geological Survey, 345 Middlefield Road, MS 999, Menlo Park, California 94025, USA (egeist@usgs.gov)

[1] The November 2000 New Ireland earthquake sequence started with a M_w = 8.0 left-lateral main shock on 16 November and was followed by a series of aftershocks with primarily thrust mechanisms. The earthquake sequence was associated with a locally damaging tsunami on the islands of New Ireland and nearby New Britain, Bougainville, and Buka. Results from numerical tsunami-propagation models of the main shock and two of the largest thrust aftershocks (M_w > 7.0) indicate that the largest tsunami was caused by an aftershock located near the southeastern termination of the main shock, off the southern tip of New Ireland (Aftershock 1). Numerical modeling and tide gauge records at regional and far-field distances indicate that the main shock also generated tsunami waves. Large horizontal displacements associated with the main shock in regions of steep bathymetry accentuated tsunami generation for this event. Most of the damage on Bougainville and Buka Islands was caused by focusing and amplification of tsunami energy from a ridge wave between the source region and these islands. Modeling of changes in the Coulomb failure stress field caused by the main shock indicate that Aftershock 1 was likely triggered by static stress changes, provided the fault was on or synthetic to the New Britain interplate thrust as specified by the Harvard CMT mechanism. For other possible focal mechanisms of Aftershock 1 and the regional occurrence of thrust aftershocks in general, evidence for static stress change triggering is not as clear. Other triggering mechanisms such as changes in dynamic stress may also have been important. The 2000 New Ireland earthquake sequence provides evidence that tsunamis caused by thrust aftershocks can be triggered by large strike-slip earthquakes. Similar tectonic regimes that include offshore accommodation structures near large strike-slip faults are found in southern California, the Sea of Marmara, Turkey, along the Queen Charlotte fault in British Columbia, and near the Alpine fault of New Zealand. Results from this study and previous stress modeling studies suggest that the likelihood of local tsunamis in these regions may significantly increase after a great strike-slip earthquake.

Components: 6031 words, 10 figures, 1 table.

Keywords: aftershocks; Coulomb failure stress; strike-slip; tsunami.

Index Terms: 3285 Mathematical Geophysics: Wave propagation (0689, 2487, 4275, 4455, 6934); 4564 Oceanography: Physical: Tsunamis and storm surges; 7250 Seismology: Transform faults.

Received 5 February 2005; **Revised** 20 May 2005; **Accepted** 2 June 2005; **Published** 21 October 2005.

Geist, E. L., and T. Parsons (2005), Triggering of tsunamigenic aftershocks from large strike-slip earthquakes: Analysis of the November 2000 New Ireland earthquake sequence, *Geochem. Geophys. Geosyst.*, *6*, Q10005, doi:10.1029/2005GC000935.

1. Introduction

[2] The 16 November 2000 M_w = 8.0 New Ireland earthquake was followed by a series of aftershocks, two with M_w > 7.0, and by a destructive tsunami. Because strike-slip earthquakes are generally inefficient in generating tsunamis, the focus of this study is to determine whether or not one of the

This paper is not subject to U.S. copyright.
Published in 2005 by the American Geophysical Union.

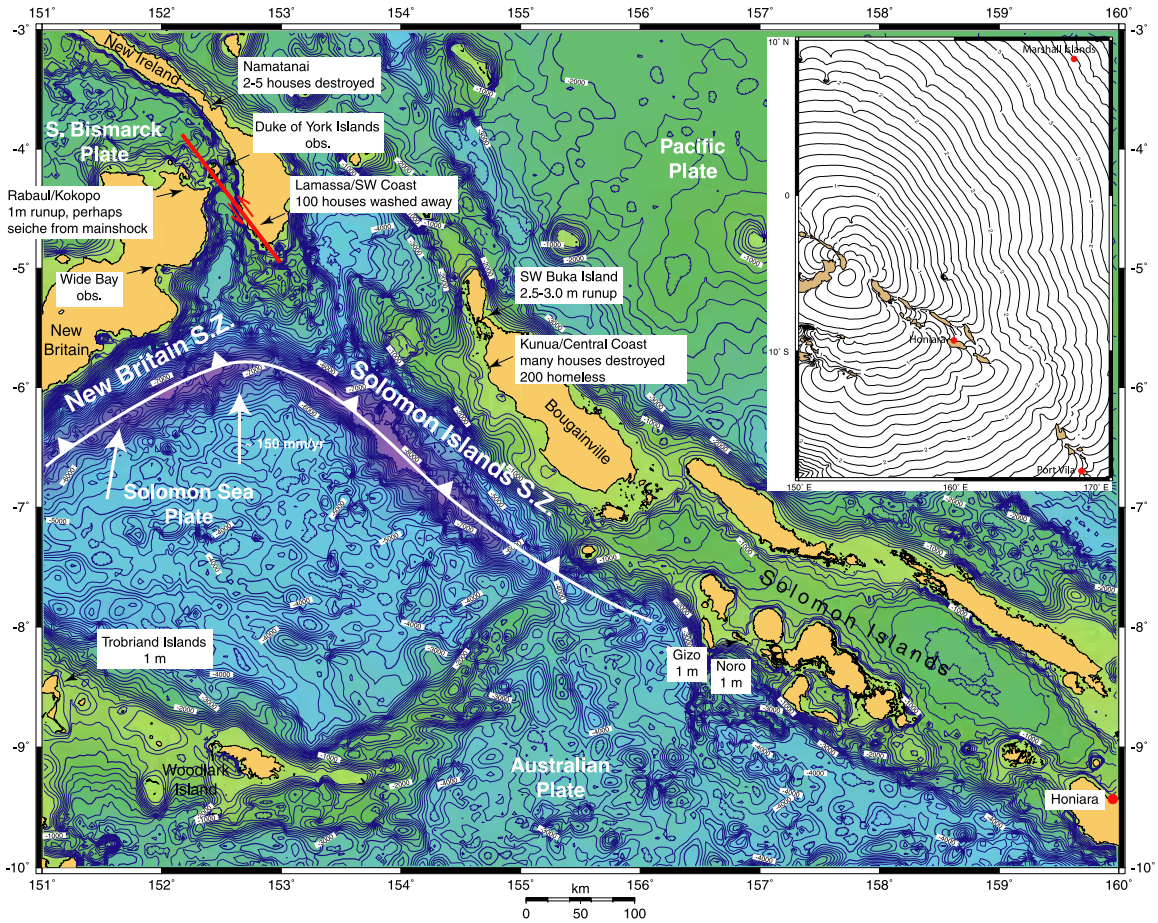

Figure 1. Location map of the New Ireland region showing major tectonic features, affected communities, and tsunami observations (obs.). Main shock fault plane shown in red. Inset: Map showing location of three tide gauge stations used in this study and tsunami travel time chart (bold contour interval: 1 hour).

large-magnitude aftershocks generated the destructive tsunami. The larger context of this question is under what conditions do large strike-slip earthquakes trigger tsunamigenic aftershocks? Better understanding of these conditions will provide increased ability to assess tsunami hazards from strike-slip earthquakes.

[3] In this study we first present background information on the earthquake sequence and tsunami observations. For the latter, the observations mainly include eyewitness observations in the near field and far-field instrumental, tide gauge records at the outer islands of the New Guinea archipelago and in the Marshall Islands (Figure 1). Tsunami modeling, using different focal mechanisms of the main shock and largest aftershocks, is performed and tested to determine consistency with the near-field observations. We then investigate static-stress changes off the southern tip of New Ireland caused by the strike-slip main shock to determine whether this is a plausible explanation for the triggering of tsunamigenic aftershocks. Finally, we consider the possibility of triggered, tsunamigenic aftershocks for other strike-slip regimes.

2. The 16 November 2000 New Ireland Earthquake Sequence

[4] The M_w = 8.0 main shock of the New Ireland earthquake sequence occurred on 16 November 2000 at 04:54:56 UTC. It was followed by 2 large ($M_w > 7$) aftershocks: one nearly three hours after the main shock (termed Aftershock 1) and one the following day (termed Aftershock 2). Numerous smaller aftershocks were mostly distributed SE of the rupture. The seismic-moment release rate for this aftershock sequence is anomalously high, in comparison to global averages (Y. Y. Kagan and H. Houston, Relation between main shock rupture process and Omori's law for aftershock moment release rate, submitted to *Journal of Geophysical Research*, 2005; hereinafter referred to as Kagan

Table 1. Seismic Moment and Best-Fit Double Couple Solutions for Main Shock and Two Largest Aftershocks

Date	M_0, Nm	M_w	Depth, km	Strike, °	Dip, °	Slip, °	Reference
16 Nov. 2000 (main shock)	3.3×10^{20}	7.6	13	306	82	79	NEIC CMT
				180	14	143	
	1.24×10^{21}	8.0	24	328	43	3	Harvard CMT
				236	88	133	
	1.6×10^{21}	8.1	35	145	84	−5	ERI[a]
16 Nov. 2000 (Aftershock 1)	1.0×10^{20}	7.3	30	288	24	122	NEIC CMT
				73	70	76	
	6.47×10^{20}	7.8	31.2	253	15	93	Harvard CMT
				70	75	89	
	1.2×10^{20}	7.3	50	84	64	89	ERI
17 Nov. 2000 (Aftershock 2)	1.4×10^{20}	7.4	37	281	32	94	NEIC CMT
				97	58	88	
	5.64×10^{20}	7.8	17.0	230	24	64	Harvard CMT
				78	68	101	
	1.2×10^{20}	7.3	55	78	57	97	ERI

[a] ERI, Earthquake Research Institute, University of Tokyo [*Yagi and Kikuchi*, 2000] (only interpreted focal plane is given).

and Houston, submitted manuscript, 2005). The seismic moment estimates and the best-fit double-couple planes for the main shock from the National Earthquake Information Center (NEIC), Harvard Centroid Moment Tensor (CMT), and Earthquake Research Institute, University of Tokyo (ERI) are given in Table 1 (see also Figure 2). Initially, it looked as though main shock occurred along the Sapom fault, although a detailed aftershock study by *Tregoning et al.* [2005] indicates that the main shock most likely occurred on the nearby Weitin fault. Analysis of the M_s = 7.2, 3 July 1985 earthquake and aftershocks by *Mori* [1989] suggests that the Sapom fault is a thrust fault that runs parallel to the Weitin fault. The Weitin fault is part of a transform system separating the North and South Bismarck plates [*Tregoning et al.*, 1998], whereas the Sapom fault is thought to be part of a remnant subduction zone [*Mori*, 1989].

[5] The discrepancy among the seismic moment estimates and fault solutions (Table 1) possibly relate to the complexity of the event that is characterized by significant amounts of shallow slip and perhaps a component of dip slip [*Park and Mori*, 2003]. Aftershock 1 (M_w = 7.3–7.8) occurred off the southern tip of New Ireland, near the cusp of the New Britain-Solomon Islands trench (Figure 2), where the Solomon Sea plate is subducting beneath the South Bismarck plate [*Tregoning et al.*, 1998]. The north-dipping plane is most likely the focal plane, though it is possible that the earthquake occurred on an upper-plate fault with an antithetic, southerly dip. Aftershock 2 (M_w = 7.3–7.8) occurred south of New Britain (Figure 2), with the NNE plane most likely the fault plane. *Rham and Das* [2003] indicate that of the 40 aftershocks that have moment tensor solutions, 11 have strike-slip mechanisms, whereas the rest had predominantly thrust mechanisms. The two largest aftershocks have magnitudes larger than predicted by Båth's Law [*Console et al.*, 2003; *Helmstetter and Sornette*, 2003], most likely because they occurred on a different fault system than the main shock (see also discussion by Kagan and Houston (submitted manuscript, 2005)).

[6] The cusp formed where the New Britain and Solomon Islands trenches join is characterized by complex seismicity, induced by a prominent change in strike of the interplate thrust. Analysis of past earthquakes suggests that seismicity and rupture patterns are controlled by contortion of the subducting Solomon Sea plate [*Kikuchi and Fukao*, 1987; *McGuire and Wiens*, 1995; *Schwartz*, 1999; *Schwartz et al.*, 1989]. An earthquake doublet on 14 July 1971 (M_w = 8.0) and 26 July 1971 (M_w = 8.1) (Figure 2) seems to have occurred on two different thrust fault strands near the cusp of the New Britain and Solomon Islands trench. *Schwartz et al.* [1989] suggest that the Solomon Island subduction zone changes strike from NW-SE in the south to a N-S strike between Bougainville and New Ireland, as indicated by the 14 July 1971 earthquake (Figure 2) and a series of smaller earthquakes from 1983–1986. It is also consistent with the mechanism of an aftershock during the most recent sequence on 18 November 2000. In

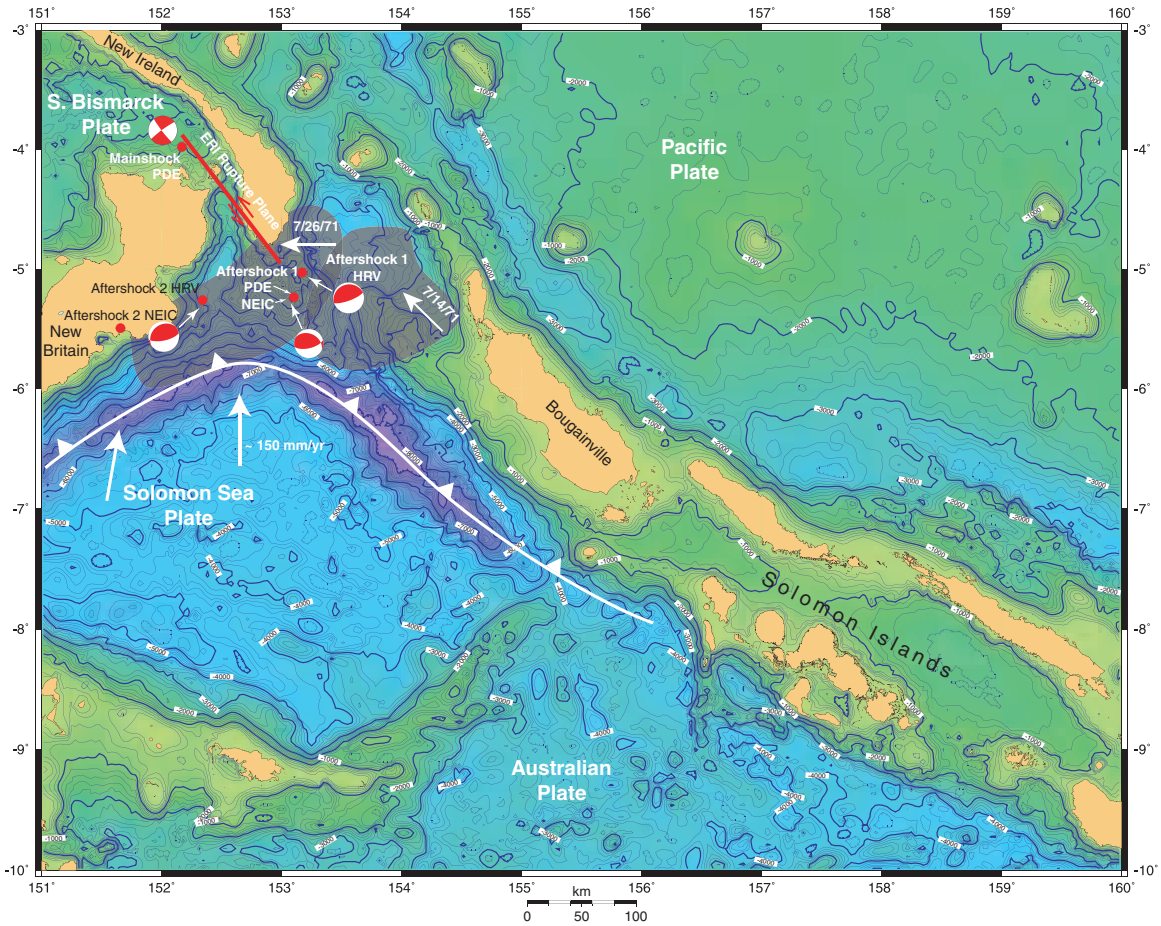

Figure 2. Locations of hypocenters and centroids for earthquakes in 2000 New Ireland earthquake sequence (solid red). Main shock: PDE and ERI rupture trace shown. Aftershock 1: PDE and NEIC and Harvard centroid locations and mechanisms shown. Aftershock 2: NEIC centroid location and Harvard centroid location and mechanism shown. Gray region is approximate extent of rupture for the 1971 doublet (M_w = 8.0 7/14/71 and M_w = 8.1 7/26/71 earthquakes); white arrows represent approximate rupture direction as interpreted by *Schwartz et al.* [1989].

contrast, the second earthquake of the 1971 doublet (26 July), started near New Ireland and propagated along the New Britain subduction zone with a ENE-WSW strike (Figure 2). The different strikes of faults near New Ireland attest to the complicated geometry of the interplate thrust. The focal mechanism of Aftershock 1 of the 2000 earthquake sequence is similar to that of the 26 July 1971 earthquake and thus most likely ruptured the New Britain part of the interplate thrust. Aftershock 2 clearly ruptured along the New Britain subduction zone and is located near a tear in the subducted plate as inferred by *McGuire and Wiens* [1995].

[7] An inversion of teleseismic body waves of the main shock from 14 stations was performed by *Yagi and Kikuchi* [2000], using the ERI reference fault model listed in Table 1. They concluded that the rupture propagated unilaterally southeast, with a maximum slip of 10 m, measured 130 km from the hypocenter (Figure 3a). Shallow slip of 5 m or greater was indicated by the inversion near where the fault cuts across New Ireland. They also performed a slip inversion of Aftershock 2, and showed that slip was concentrated in the center of the rupture zone, just downdip of the hypocenter (Figure 3b).

3. Tsunami Observations

[8] Most of the tsunami damage arising from the New Ireland earthquake sequence was concentrated on Bougainville and Buka Islands and in southern New Ireland (Figure 1). On Bougainville, many houses were destroyed by the tsunami, and a 2.5–3 m runup was reported on SW Buka Island. One hundred homes and a church were destroyed with a reported 3 m runup at Lamassa, located on

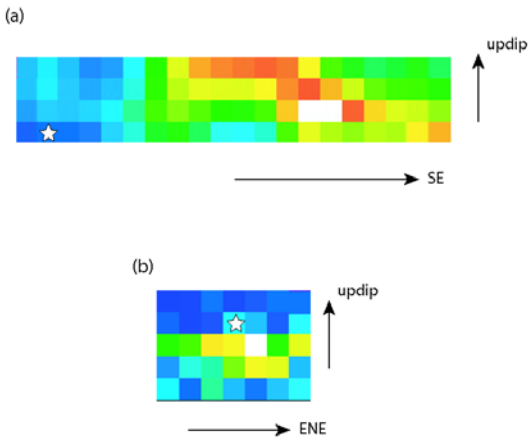

Figure 3. Slip distribution for (a) the main shock and (b) Aftershock 2 determined by *Yagi and Kikuchi* [2000]. Light colors indicate higher slip. Maximum slip is 9.7 m and 1.1 m for Figures 3a and 3b, respectively. Fault cell size is 10 km and 20 km for Figures 3a and 3b, respectively. Star indicates location of hypocenter.

the southern tip of New Ireland. Tsunami destruction was reported near Namatanai (located near the center of New Ireland), the Duke of York Islands (between New Ireland and New Britain), and Wide Bay, NE New Britain. One meter tsunami runups were observed at the Trobriand Islands, south of New Britain and at Gizo and Noro in the western province of the Solomon Islands (Figure 1). Some eyewitnesses on along the southern coast of New Ireland reported seeing tsunami waves minutes after the main shock (J. Mori, written communication, 2005), indicating that the main shock produced significant local tsunami waves. Observations of unusual wave activity were also reported in Rabaul harbor and ascribed to a seiche [*International Tsunami Information Center* (*ITIC*), 2000; *Lander et al.*, 2003], although these observations are also consistent with tsunami generation that includes large horizontal motions from the main shock as explained below.

[9] Instrumental records of the tsunami from tide-gauge records in the Solomon Islands and Vanuatu are available through the National Tidal Facility of Australia (Figure 4). The tsunami was also recorded by a tide gauge station on the Marshall Islands operated by NOAA/NOS (Figure 5). Tsunami arrival times corresponding to sources from the main shock and Aftershock 1 (MS and AS1, respectively) are indicated in Figures 4 and 5, using travel time modeling based on ETOPO2 bathymetry [*Smith and Sandwell*, 1997]. The Solomon Islands and Vanuatu tide gauge stations indicate anomalous wave activity following the predicted arrival time of tsunamis following the main shock, but the lack of a prominent first arrival makes it difficult to ascertain the onset of tsunami waves. For the case of Honiara (Solomon Islands), tsunami waves were greatly attenuated as they passed through the western island chain (Figure 1).

[10] The Marshall Islands tide gauge station, located approximately 2,200 km to the NE of New Ireland, indicates unusual wave activity beginning at approximately the predicted arrival time of tsunami waves from the main shock, and smaller waves arriving at the predicted time of the aftershock are also noticeable (Figure 5). Although the relatively higher amplitude of the main shock tsunami at the Marshall Islands station is consistent with numerical modeling results (below), the Marshall Islands station is near a tsunami nodal azimuth [*Ward*, 1982] for both the strike-slip main shock and dip-slip Aftershock 1. It appears from the instrumental records that tsunami waves were generated from both the main shock and Aftershock 1, although without first performing numerical simulations (as presented below), it is

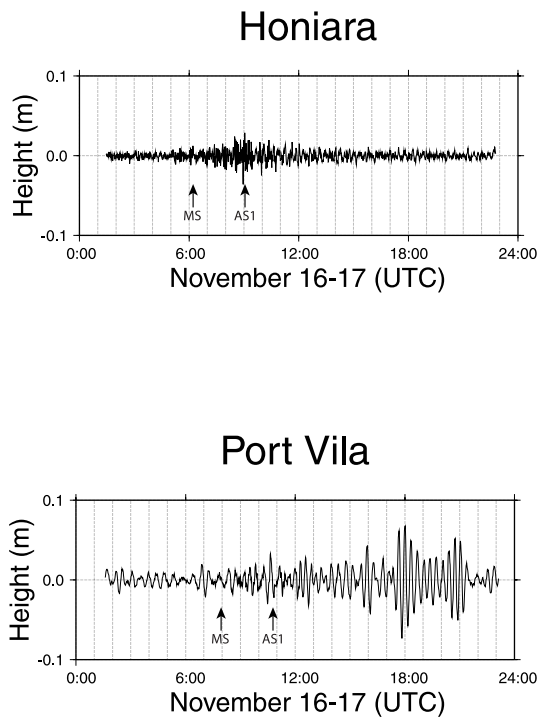

Figure 4. Tide gauge records from the National Tidal Facility of Australia from Honiara (Solomon Islands) and Port Vila (Vanuatu) filtered to remove the tidal component. MS and AS1 indicated the predicted arrival time of tsunamis generated by the main shock and Aftershock 1, respectively. Sample rate is 1 minute.

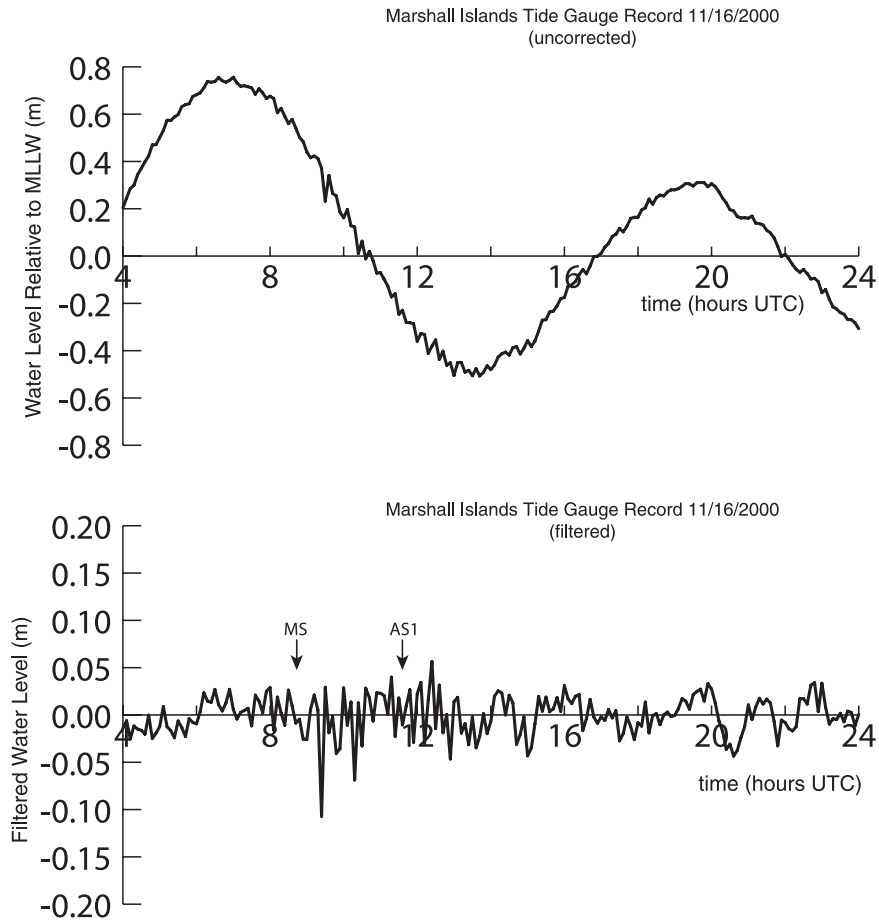

Figure 5. Kwajalein, Marshall Islands tide gauge record (NOAA/NOS) filtered to remove the tidal component. MS and AS1 indicated the predicted arrival time of tsunamis generated by the main shock and Aftershock 1, respectively. Sample rate is 6 minutes.

unclear which source caused the damaging near-field tsunami.

4. Tsunami Modeling

[11] From data in the previous sections, it is evident that tsunami travel time modeling alone cannot determine the mechanism whereby the main shock and Aftershock 1 caused the observed tsunami. In this section, we model the tsunami produced from the main shock and both aftershocks to determine if these tsunamis can explain the near-field runup observations (Figure 1).

[12] The initial tsunami wave field is traditionally computed from the coseismic vertical displacement of the seafloor. However, because of the large horizontal displacements associated with the main shock in regions of steep bathymetry, we also include the displacement of the water column from these horizontal movements as explained by *Tanioka and Satake* [1996]. The slip distribution derived from *Yagi and Kikuchi* [2000] (Figure 3a) is used to calculate both the horizontal and vertical coseismic displacement fields by superposition [*Satake*, 1993] of point-source dislocations using the expressions of *Okada* [1985]. The additional displacement of the water column (u_h) caused by the horizontal displacement field (u_x, u_y) given by *Tanioka and Satake* [1996] is

$$u_h = u_x \frac{\partial h}{\partial x} + u_y \frac{\partial h}{\partial y},$$

where h is the water depth (positive). The 2 components of the initial tsunami wave field are shown in Figure 6a and 6b, with the total initial tsunami wave field shown in Figure 6c. The effect of the horizontal displacement is to create additional elevation waves off the southeast coast of New Britain, north of Wide Bay, and additional depression waves off the southeast coast of New Ireland (Figure 6b). The effect of including

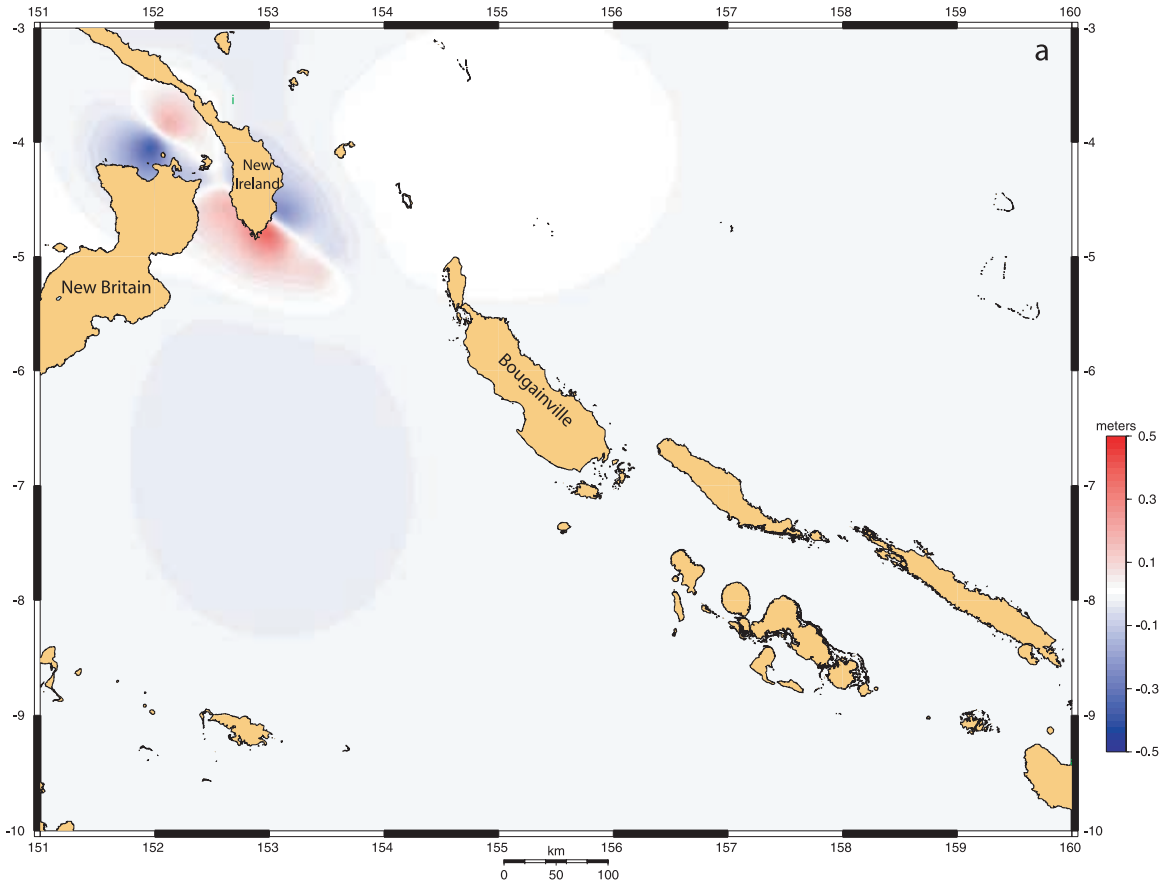

Figure 6. Initial tsunami wave field for main shock showing different components of water displacements: (a) coseismic vertical displacement only; (b) displacement of water calculated from coseismic horizontal displacement and bathymetric gradient; (c) total initial wave field, combining Figures 6a and 6b.

horizontal displacement on the initial tsunami wave field is much less for the dip-slip aftershocks.

[13] For Aftershock 1, a discretized slip distribution corresponding to an ideal crack is used [*Geist and Dmowska*, 1999] since the slip distribution is not known. The tsunami from both nodal planes of Aftershock 1 are modeled, since it is not certain that the earthquake occurred on the New Britain interplate thrust. For Aftershock 2, the slip distribution from the inversion of *Yagi and Kikuchi* [2000] (Figure 3b) is used to compute the initial tsunami wave field.

[14] Wave propagation is modeled using a finite difference approximation to the linear-long wave equation [*Satake*, 2002]. ETOPO2 bathymetry interpolated onto a 1-minute grid was used in the propagation calculations. Modeled propagation stopped at the 50 m isobath, where perfect-reflection boundary conditions are assumed. Shallower than approximately 50 m water depth, nonlinear effects are likely to become important, depending on the wave amplitude. For the open-ocean boundaries, a radiant boundary condition is used. A time step of 4.4 seconds was used to ensure numerical stability according to the Courant-Friedrichs-Lewy (CFL) criterion for the greatest water depth in the model domain. Wave propagation was calculated for a duration of 146 minutes after each earthquake.

[15] The maximum tsunami amplitude for each of the earthquakes (2 for each nodal plane of Aftershock 1) is presented in Figure 7 (note change in amplitude scale). To approximately convert offshore tsunami amplitudes to runup, an empirical amplification is often used [*Imamura et al.*, 1993; *Shuto*, 1991]. An amplification factor of 2 is commonly assumed, but the value depends on wave characteristics and bathymetry. For the sites where tsunami damage was observed, the tsunami amplitudes are highest for the Aftershock 1 source (Figures 7b and 7c). Although both nodal planes are consistent with the approximate nature of the runup observations,

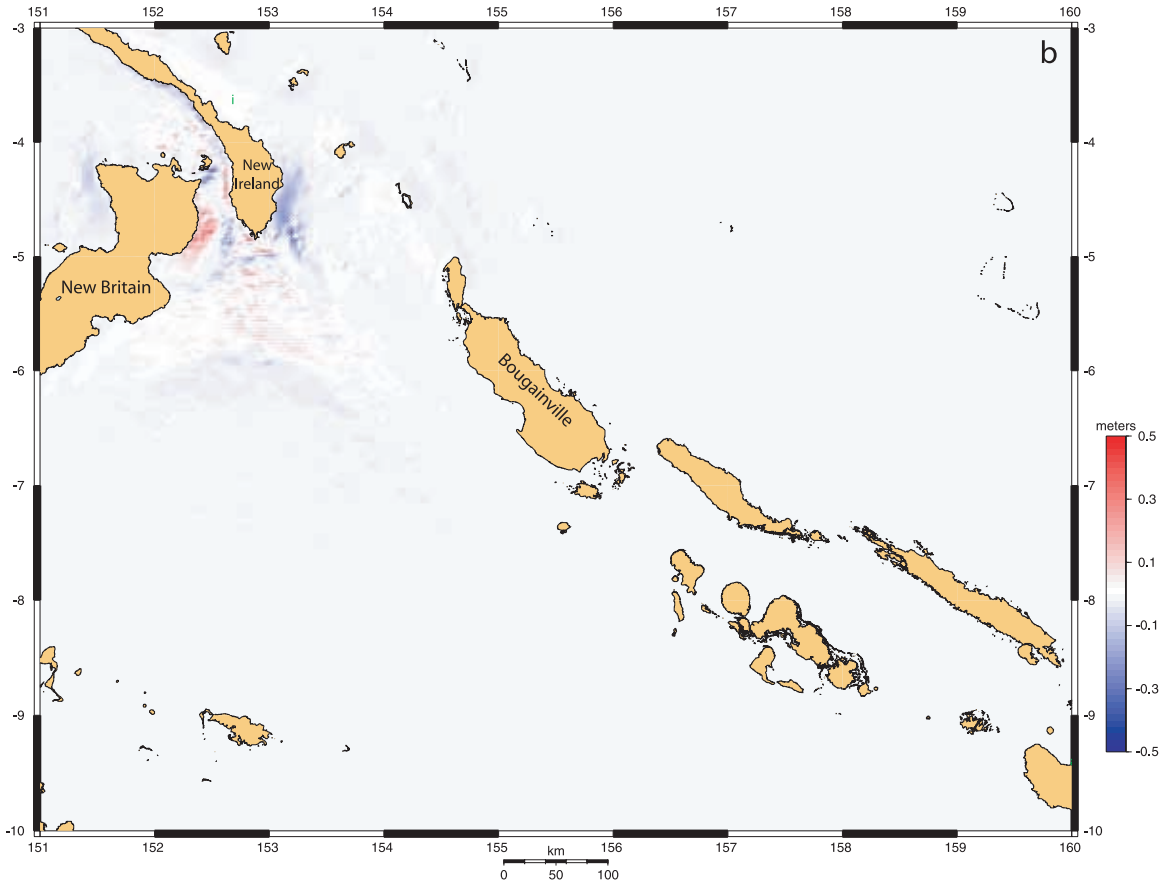

Figure 6. (continued)

the tsunami from the steeply dipping nodal plane (nodal plane 2) produces higher tsunami amplitudes, relating to a higher proportion of vertical displacement for this type of mechanism [*Geist*, 1999]. Of particular interest in explaining the runup observations on Bougainville and Buka Islands is a ridge wave [*Satake et al.*, 1992] that follows a bathymetric high trending NW-SE, to the east of the central coast of Bougainville (Figure 8). A ridge wave results from refraction and focusing of long-wave energy during propagation [*Mei*, 1989]. The ridge wave can be observed in the animation of tsunami wave propagation from Aftershock 1, nodal plane 2 (Animation 1). An important model result is that the open-ocean tsunami amplitudes in the NE part of the model domain are slightly larger for the main shock than for any of the aftershocks, consistent with the relative amplitude of the main shock and Aftershock 1 tsunamis from the Marshall Islands tide gauge record. Also, the tsunami amplitudes arising from the main shock along the southern coast of New Ireland most likely would have been observable (>1 m) and therefore consistent with the eyewitness observations.

5. Triggering Mechanisms

[16] Because the aftershocks occur on different fault systems and because they appear to have anomalously large magnitudes with respect to typical aftershock sequences (Kagan and Houston, submitted manuscript, 2005), we explore possible triggering mechanisms for these events. A variety of triggering mechanisms have been proposed for aftershocks, and for earthquakes that are distant in time and space from a main shock. *Parsons* [2002] calculated that ~61% of earthquakes with $M_s \geq 5$ in the Harvard CMT catalog were associated with static stress increases from nearby $M_s \geq 7$ earthquakes. An often-used triggering criterion is the change in the Coulomb failure stress (ΔCFS), defined by

$$\Delta CFS \equiv \Delta\tau_{slip} + \mu(\Delta\sigma_n + \Delta P),$$

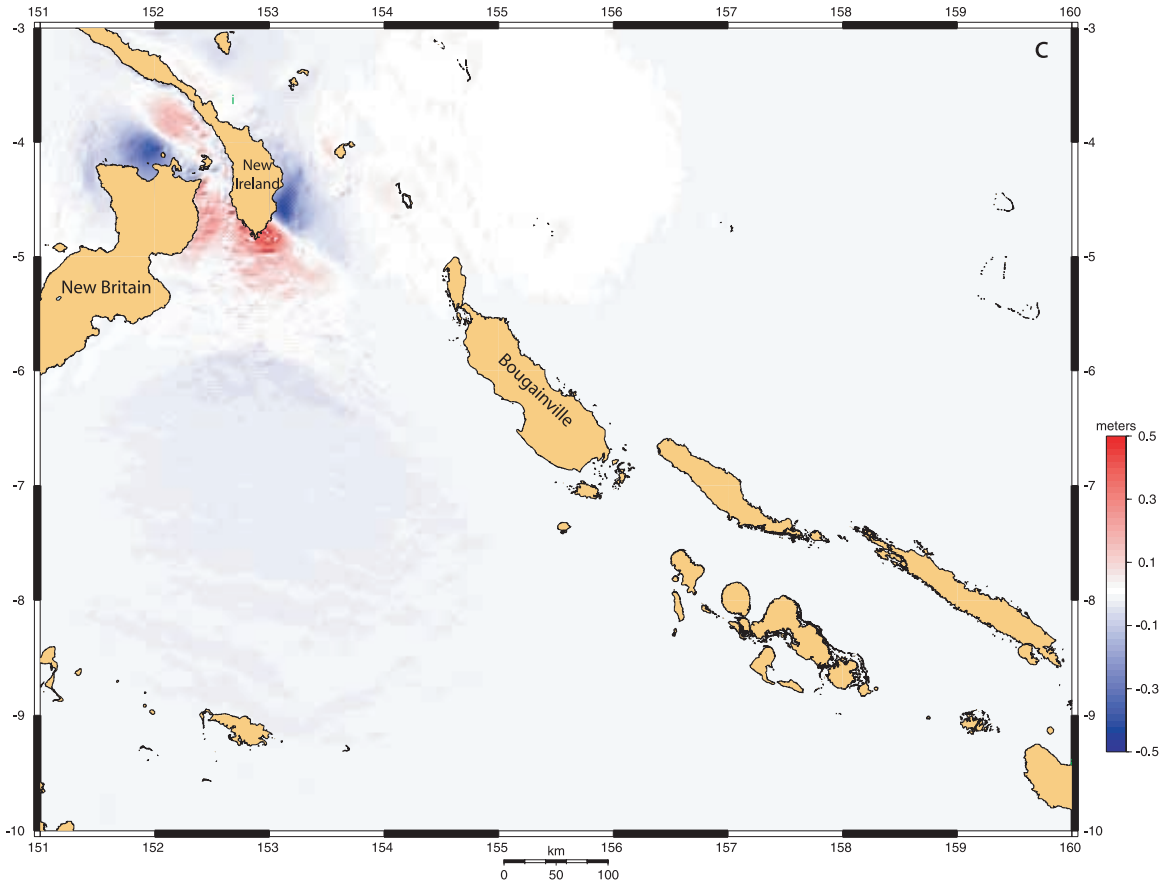

Figure 6. (continued)

where $\Delta\tau_{slip}$ is the change in shear stress resolved in the direction of slip and $\Delta\sigma_n$ change in normal stress for the receiving fault, μ is the coefficient of friction and ΔP is the change in pore pressure. As an approximation, the equation for ΔCFS can be written as

$$\Delta CFS \approx \Delta\tau_{slip} + \mu'\Delta\sigma_n,$$

where μ' is the effective coefficient of friction. Earthquakes correlated with positive ΔCFS occur above the background rate of seismicity and sometimes at distances greater than 240 km from the main shock [*Parsons*, 2002]. A good example of ΔCFS triggering is the progression of seven $\mathbf{M} \geq 6.7$ earthquakes along the North Anatolian fault in Turkey since 1939, in which all but one event was calculated to have promoted the next [*Stein et al.*, 1997]. In subduction tectonic settings, *Taylor et al.* [1998], and *ten Brink and Lin* [2004] show how strike-slip events in the overriding plate can be triggered by large subduction zone earthquakes. The ΔCFS triggering mechanism is a static or long-term transient mechanism. In addition, there are a number of dynamic triggering mechanisms that involve oscillating changes in stress from the propagation of seismic waves [e.g., *Gomberg et al.*, 2001; *Kilb et al.*, 2000].

[17] For the New Ireland earthquake sequence, change in the static stress field is calculated using the main shock slip distribution determined from the inversion of teleseismic body waves by *Yagi and Kikuchi* [2000] (Figure 3). In Figures 9 and 10, ΔCFS is resolved along the nodal planes of Aftershock 1 for both the NEIC (Figure 9) and Harvard CMT (Figure 9) solutions using the DLC code [*Simpson and Reasenberg*, 1994] based on subroutines of *Okada* [1992]. The finite rupture area is scaled according to the estimated seismic moment of Aftershock 1 (Table 1) and in each case, the centroid is assumed to occur in the center of the rupture plane. For each nodal plane, three different values for the effective coefficient of friction (μ') are used. The Preliminary Determination of Epicenter (PDE) for Aftershock 1 is projected onto each plane where possible. The largest regions of positive ΔCFS occur using the NEIC

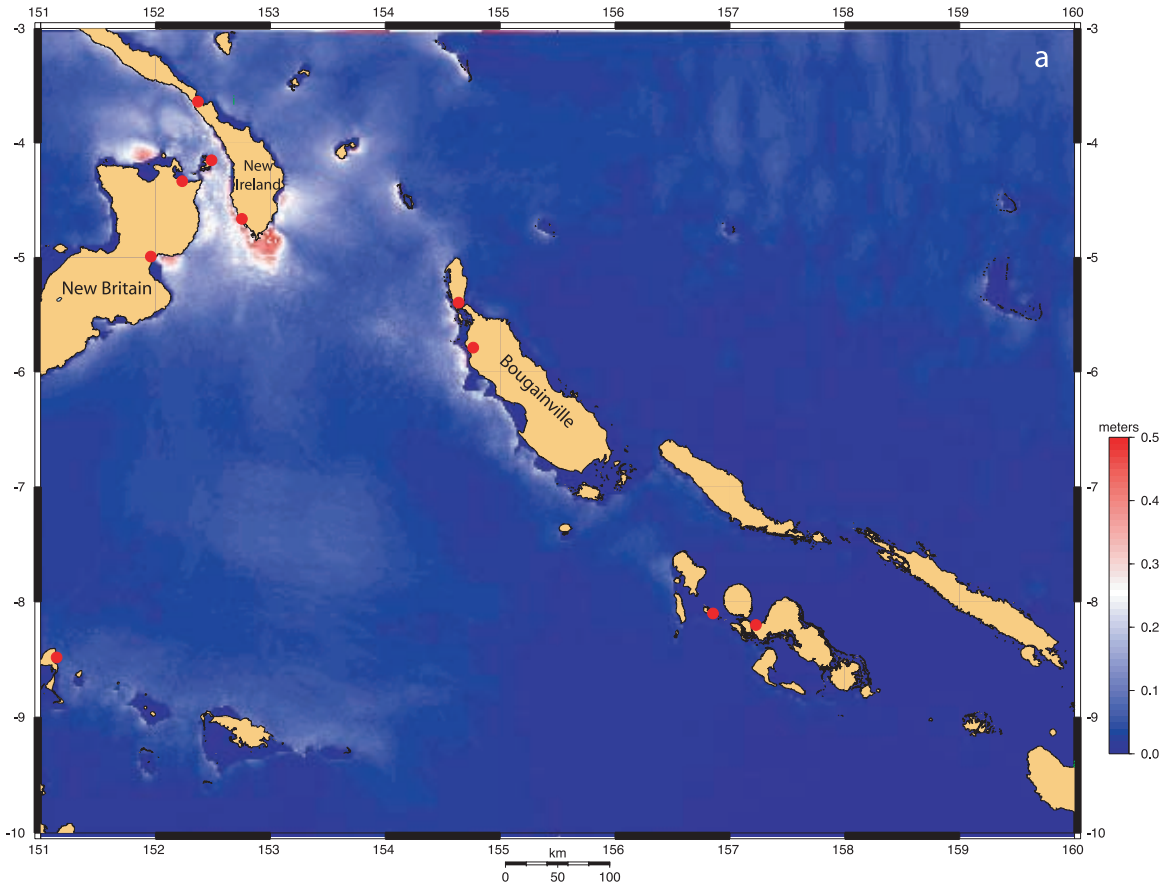

Figure 7. Maximum tsunami amplitude for the following earthquakes: (a) main shock; (b) Aftershock 1, nodal plane 1 (shallow-dipping thrustplane); (c) Aftershock 1, nodal plane 2 (steeply-dipping plane); (d) Aftershock 2 (shallow-dipping plane). Note that the wave amplitude scale for the main shock and Aftershock 2 (Figures 7a and 7d) is different from that for the 2 nodal planes of Aftershock 1 (Figures 7b and 7c). Red dots indicate locations of tsunami damage/observations (see Figure 1).

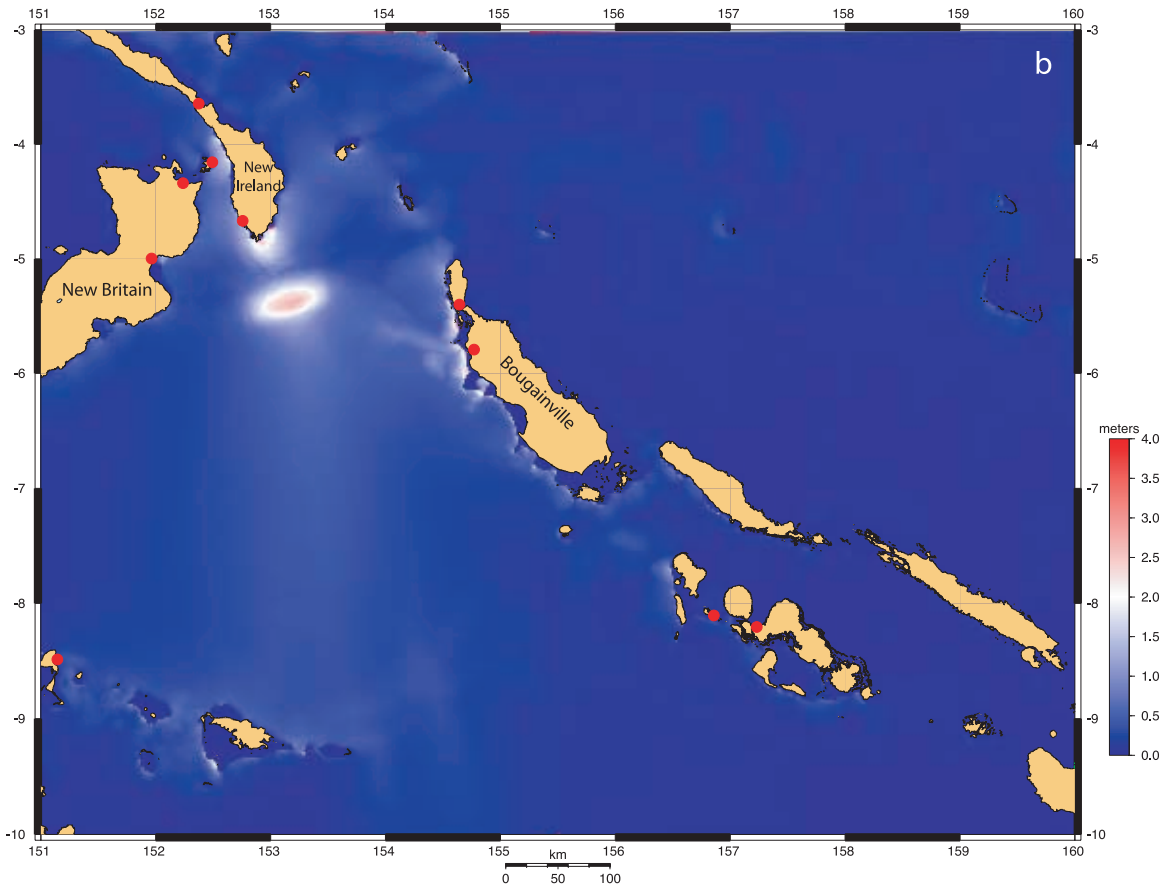

Figure 7. (continued)

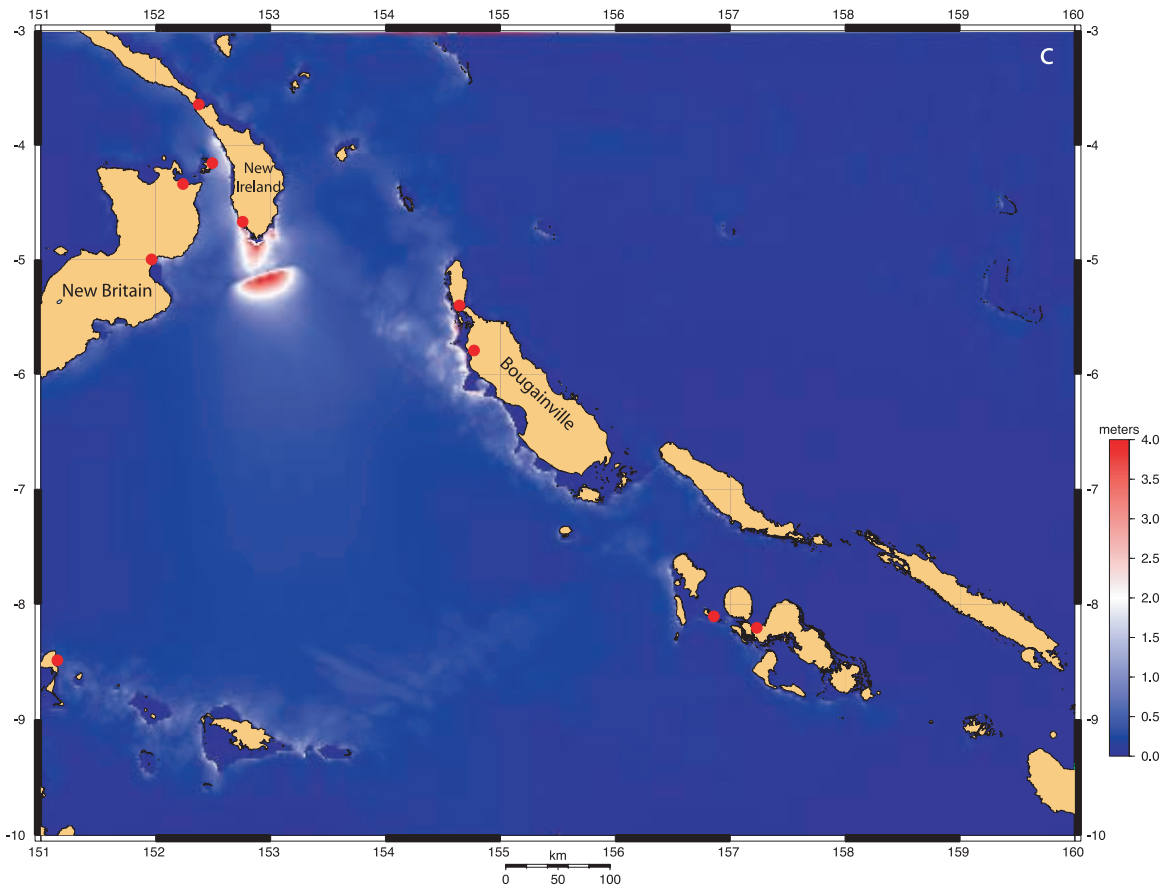

Figure 7. (continued)

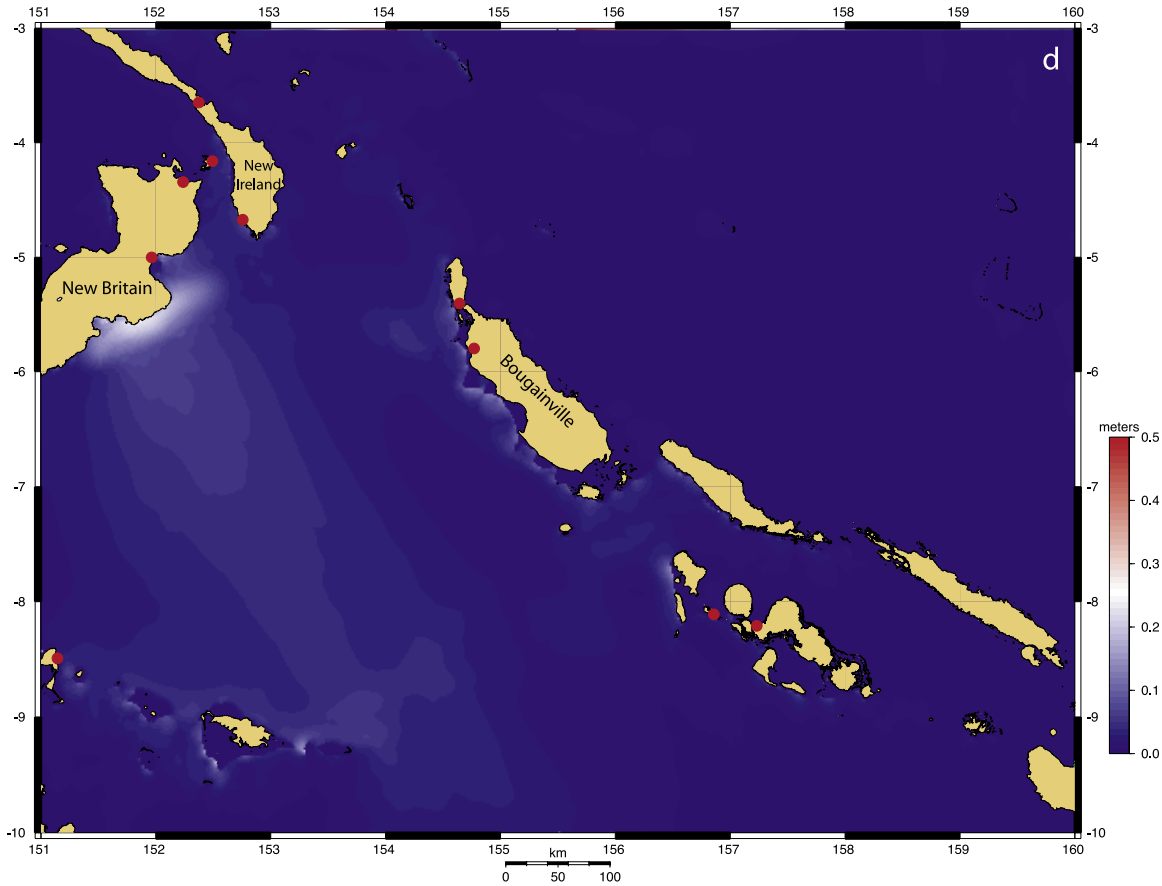

Figure 7. (continued)

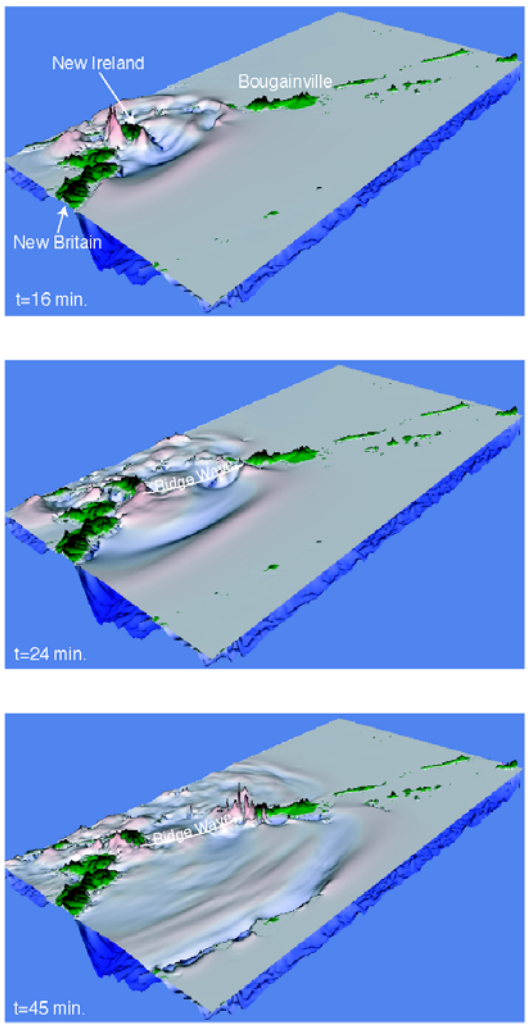

Figure 8. Snapshots of tsunami simulation using the Aftershock 1, nodal plane 2 source. Propagation of ridge wave shown toward Buka and Bougainville Islands, where most of the damage was observed (Figure 1).

nodal plane 2 (antithetic to the New Britain interplate thrust) with $\mu' = 0$ and for the Harvard nodal plane 1 (on or synthetic to the New Britain interplate thrust). If one were to assume that the earthquake occurred on the New Britain interplate thrust specified by the Harvard mechanism (Figure 10a), then static stress change is a likely explanation for the triggering mechanism Aftershock 1. However, because Aftershock 1 is very close to the rupture termination of the main shock, the resolved stress field is strongly heterogeneous, especially for the steeply dipping nodal plane 2 (Figure 9b and 10b). Whereas Aftershocks 1 and 2 are likely in regions of positive ΔCFS, the more regional occurrence of thrust aftershocks along the New Britain subduction zone [*Rham and Das*, 2003] suggests that dynamic triggering mechanisms may also be important.

6. Implications for Tsunami Hazards in Strike-Slip Regimes

[18] The main conclusion of this study is that the 2000 New Ireland earthquake sequence provides evidence that tsunamigenic dip-slip earthquakes can be triggered by large strike-slip earthquakes. This conclusion has direct implications for tsunami hazards in strike-slip regimes, and is supported by observations globally. In Turkey, the right-lateral North Anatolian fault makes several releasing steps that are associated with normal faults as it trends beneath the Sea of Marmara near Istanbul [e.g., *Armijo et al.*, 1999]. Seafloor displacements or landslides associated with North Anatolian fault earthquakes have caused more than 30 tsunamis over the past 2000 years [*Hébert et al.*, 2003; *Yalciner et al.*, 2002]. In New Zealand, major tsunami events have been associated with ruptures along the right-lateral oblique Alpine fault system [*Downes and Stirling*, 2001; *Goff et al.*, 2000]. A tsunamigenic (maximum tide gauge reading of 20 cm) $M_w = 6.3$ earthquake occurred in 2001 on an adjacent thrust fault to the right-lateral Queen Charlotte fault, which marks the Pacific-North American plate boundary offshore of British Columbia [*Rogers et al.*, 2002].

[19] In densely populated southern California, the onshore San Andreas fault is associated with the compressional regime of the western Transverse Ranges and the Channel Island thrust system, offshore Santa Barbara. For example, there is evidence [*Fisher et al.*, 2003; *Seeber and Sorlien*, 2000; *Tsutsumi et al.*, 2001] that recent motion is evident along the compressional Dume fault beneath Santa Monica Bay, east of the Channel Islands thrust system. As a possible analog of the 2000 New Ireland earthquake sequence, *Deng and Sykes* [1996] proposed that the 21 December 1812 Santa Barbara earthquake was triggered by an earthquake on the San Andreas fault 13 days earlier. The Santa Barbara earthquake is associated with a tsunami [*Borrero et al.*, 2001], though it is unclear whether an offshore landslide triggered by the earthquake also contributed to tsunami generation [*Lee et al.*, 2004].

[20] *Deng and Sykes* [1996] show ΔCFS from a great earthquake along the Wrightwood segment of the San Andreas fault (the proposed 1812 trigger earthquake) and a future scenario in which a great

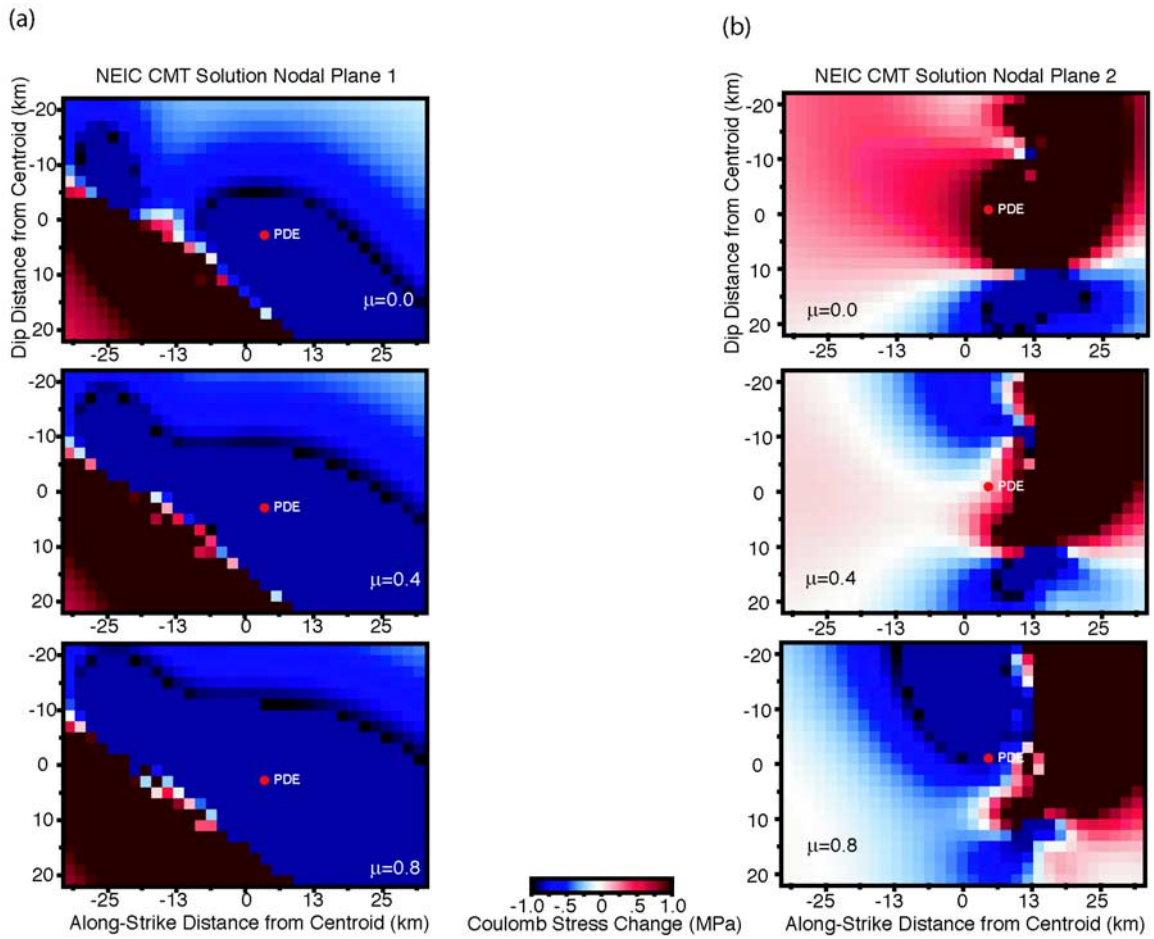

Figure 9. Change in the Coulomb failure stress (ΔCFS) caused by the main shock in the plane of Aftershock 1, using either (a) nodal plane 1 or (b) nodal plane 2 from the NEIC mechanism as the receiving fault. For each nodal plane, 3 different values of the effective coefficient of friction are shown. PDE location for Aftershock 1 projected onto each plane.

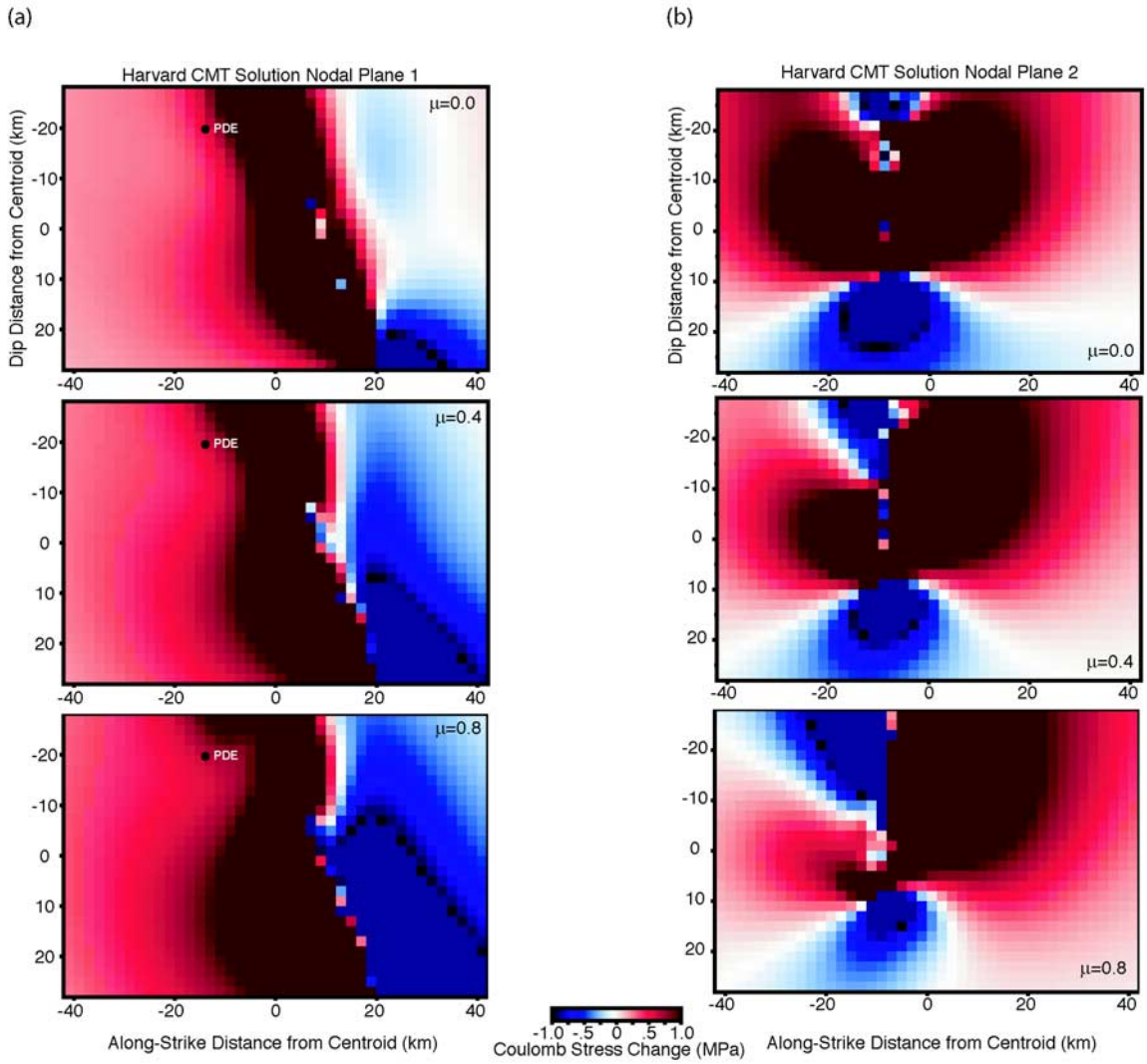

Figure 10. Change in the Coulomb failure stress (ΔCFS) caused by the main shock in the plane of Aftershock 1, using either (a) nodal plane 1 or (b) nodal plane 2 from the Harvard CMT mechanism as the receiving fault. For each nodal plane, 3 different values of the effective coefficient of friction are shown. PDE location for Aftershock 1 projected onto nodal plane 1 (a). (PDE cannot be projected onto nodal plane 2.)

earthquake ruptures the San Bernadino and Coachella Valley segments of the San Andreas fault. In both cases, regions of positive ΔCFS include the Channel Islands thrust system and Santa Monica Bay for receiver faults with an oblique thrust mechanism (strike = 280°). These results indicate an increase in the likelihood of thrust earthquakes, potentially tsunamigenic, occurring offshore the heavily urbanized areas of southern California following a great earthquake on the southern San Andreas fault.

7. Conclusions

[21] Although the sequence of earthquakes and tsunamis on 16–17 November 2000 in the New Ireland region is complex, results from numerical modeling indicate that the damaging tsunami on Bougainville was caused by the M_w = 7.3–7.8 reverse faulting aftershock that occurred 3 hours after the main shock (Aftershock 1). It is important to also note that the strike-slip main shock also created significant tsunami wave heights. At regional distances (Solomon Islands, Vanuatu) and in the far-field (Marshall Islands), tsunamis from both the main shock and Aftershock 1 are evident, as indicated by tide gauge records and travel time modeling. If one assumes that the plane of faulting was on, or synthetic to, the New Britain interplate thrust with parameters specified by the Harvard CMT catalog, then an increase in the static Coulomb failure stress caused by the main shock is the

likely mechanism. For other nodal plane possibilities and the occurrence of regional thrust aftershocks, however, triggering is not as clear and may involve both static and dynamic mechanisms. The likelihood of offshore tsunamis may increase significantly following a great strike-slip earthquake in other strike-slip regimes such as southern California.

Acknowledgments

[22] This study greatly benefited from discussions with Michael Blackford and Kenji Hirata (JAMSTEC). Slip inversion results and filtered south Pacific tide gauge records were generously provided by Yuji Yagi (ERI, University of Tokyo) and Paul Davill (National Tidal Facility, Australia), respectively. Constructive reviews of the manuscript by Jim Mori, Kenji Satake, Greg Beroza, Michael Fisher, and Robert Kayen are much appreciated. Maps were constructed using Generic Mapping Tools (GMT) [*Wessel and Smith*, 1995].

References

Armijo, R., B. Meyer, A. Hubert, and A. Barka (1999), Westward propagation of the North Anatolian fault into the northern Aegean: Timing and kinematics, *Geology*, *27*, 267–270.

Borrero, J. C., J. F. Dolan, and C. E. Synolakis (2001), Tsunamis within the eastern Santa Barbara Channel, *Geophys. Res. Lett.*, *28*, 643–647.

Console, R., A. M. Lombardi, M. Murru, and D. Rhoades (2003), Båth's law and the self-similarity of earthquakes, *J. Geophys. Res.*, *108*(B2), 2128, doi:10.1029/2001JB001651.

Deng, J., and L. R. Sykes (1996), Triggering of 1812 Santa Barbara earthquake by a great San Andreas shock: Implications for future seismic hazard in southern California, *Geophys. Res. Lett.*, *23*, 1155–1158.

Downes, G. L., and M. W. Stirling (2001), Groundwork for development of a probabilistic tsunami hazard model for New Zealand, paper presented at International Tsunami Symposium 2001, Int. Union of Geod. and Geophys. Tsunami Comm., Seattle, Washington.

Fisher, M. A., W. R. Normark, R. G. Bohannon, R. W. Sliter, and A. J. Calvert (2003), Geology of the continental margin beneath Santa Monica Bay, southern California, from seismic-reflection data, *Bull. Seismol. Soc. Am.*, *93*, 1955–1983.

Geist, E. L. (1999), Local tsunamis and earthquake source parameters, *Adv. Geophys.*, *39*, 117–209.

Geist, E. L., and R. Dmowska (1999), Local tsunamis and distributed slip at the source, *Pure Appl. Geophys.*, *154*, 485–512.

Goff, J. R., H. L. Rouse, S. L. Jones, B. W. Hayward, U. Cochrane, W. McLea, W. W. Dickinson, and M. S. Morley (2000), Evidence for an earthquake and tsunami about 3100 to 3400 years ago, and other catastrophic salt water inundations recorded in a coastal lagoon, New Zealand, *Mar. Geol.*, *170*, 233–251.

Gomberg, J., P. A. Reasenberg, P. Bodin, and R. A. Harris (2001), Earthquake triggering by seismic waves following the Landers and Hector mine earthquakes, *Nature*, *411*, 462–466.

Hébert, H., F. Schindelé, Y. Altinok, and B. Alpar (2003), Tsunami modeling in the Marmara Sea (Turkey): Risk assessment and study of active faulting, *Geophys. Res. Abstr.*, *5*, 10,100.

Helmstetter, A., and D. Sornette (2003), Båth's law derived from the Gutenberg-Richter law and from aftershock properties, *Geophys. Res. Lett.*, *30*(20), 2069, doi:10.1029/2003GL018186.

Imamura, F., N. Shuto, S. Ide, Y. Yoshida, and K. Abe (1993), Estimate of the tsunami source of the 1992 Nicaraguan earthquake from tsunami data, *Geophys. Res. Lett.*, *20*, 1515–1518.

International Tsunami Information Center (ITIC) (2000), Summary of Pacific Basin earthquakes occurring October–November 2000, in *Tsunami Newsletter*, p. 2, Honolulu.

Kikuchi, M., and Y. Fukao (1987), Inversion of long-period P-waves from great earthquakes along subduction zones, *Tectonophysics*, *144*, 231–247.

Kilb, D. L., J. Gomberg, and P. Bodin (2000), Triggering of earthquake aftershocks by dynamic stresses, *Nature*, *408*, 570–574.

Lander, J. F., L. S. Whiteside, and P. A. Lockridge (2003), Two decades of global tsunamis: 1982–2002, *Sci. Tsunami Hazards*, *21*, 3–88.

Lee, H., W. R. Normark, M. A. Fisher, H. G. Greene, B. D. Edwards, and J. Locat (2004), Timing and extent of submarine landslides in southern California, paper presented at Offshore Technology Conference, OTC Program Comm., Houston, Tex.

McGuire, J. J., and D. A. Wiens (1995), A double seismic zone in New Britain and the morphology of the Solomon Plate at intermediate depths, *Geophys. Res. Lett.*, *22*, 1965–1968.

Mei, C. C. (1989), *The Applied Dynamics of Ocean Surface Waves*, 740 pp., World Sci., Hackensack, N. J.

Mori, J. (1989), The New Ireland earthquake of July 3, 1985 and associated seismicity near the Pacific-Solomon Sea-Bismarck Sea triple junction, *Phys. Earth Planet. Inter.*, *55*, 144–153.

Okada, Y. (1985), Surface deformation due to shear and tensile faults in a half-space, *Bull. Seismol. Soc. Am.*, *75*, 1135–1154.

Okada, Y. (1992), Internal deformation due to shear and tensile faults in half-space, *Bull. Seismol. Soc. Am.*, *82*, 1018–1040.

Park, S., and J. Mori (2003), Triggering of large earthquake in the 2000 New Ireland, Papua New Guinea sequence, paper presented at 2003 International Union of Geology and Geophysics General Assembly, Sapporo, Japan.

Parsons, T. (2002), Global Omori law decay of triggered earthquakes: Large aftershocks outside the classical aftershock zone, *J. Geophys. Res.*, *107*(B9), 2199, doi:10.1029/2001JB000646.

Rham, D. J., and S. Das (2003), Triggering of thrust aftershocks on the New Britain trench by the November 16, 2000 MW 8.0 New Ireland strike-slip earthquake, paper presented at 2003 International Union of Geology and Geophysics General Assembly, Sapporo, Japan.

Rogers, G., J. Ristau, A. Bird, A. B. Rabinovich, V. V. Titov, and R. Thomson (2002), The 12 October 2001 Queen Charlotte Islands earthquake and tsunami, *Seismol. Res. Lett.*, *73*, 259.

Satake, K. (1993), Depth distribution of coseismic slip along the Nankai trough, Japan, from joint inversion of geodetic and tsunami data, *J. Geophys. Res.*, *98*, 4553–4565.

Satake, K. (2002), Tsunamis, in *International Handbook of Earthquake and Engineering Seismology*, edited by W. H. K. Lee et al., pp. 437–451, Elsevier, New York.

Satake, K., Y. Yoshida, and K. Abe (1992), Tsunami from the Mariana earthquake of April 5, 1990: Its abnormal propagation and implications for tsunami potential from outer-rise earthquakes, *Geophys. Res. Lett.*, *19*, 301–304.

Schwartz, S. Y. (1999), Noncharacteristic behavior and complex recurrence of large subduction zone earthquakes, *J. Geophys. Res.*, *104*, 23,111–123,125.

Schwartz, S. Y., T. Lay, and L. J. Ruff (1989), Source process of the great 1971 Solomon Islands doublet, *Phys. Earth Planet. Inter.*, *56*, 294–310.

Seeber, L., and C. Sorlien (2000), Listric thrusts in the western Transverse Ranges, California, *Geol. Soc. Am. Bull.*, *112*, 1067–1079.

Shuto, N. (1991), Numerical simulation of tsunamis—Its present and near future, *Nat. Hazards*, *4*, 171–191.

Simpson, R. W., and P. A. Reasenberg (1994), Earthquake-induced static-stress changes on central California faults, *U.S. Geol. Surv. Prof. Pap.*, *55*, 89 pp.

Smith, W. H. F., and D. T. Sandwell (1997), Global seafloor topography from satellite altimetry and ship depth soundings, *Science*, *277*, 1957–1962.

Stein, R. S., A. A. Barka, and J. H. Dieterich (1997), Progressive failure on the North Anatolian fault since 1939 by earthquake stress triggering, *Geophys. J. Int.*, *128*, 594–604.

Tanioka, Y., and K. Satake (1996), Tsunami generation by horizontal displacement of ocean bottom, *Geophys. Res. Lett.*, *23*, 861–865.

Taylor, M. A. J., R. Dmowska, and J. R. Rice (1998), Upper plate stressing and seismicity in the subduction earthquake cycle, *J. Geophys. Res.*, *103*, 24,523–524,542.

ten Brink, U., and J. Lin (2004), Stress interaction between subduction earthquakes and forearc strike-slip faults: Modeling and application to the northern Caribbean plate boundary, *J. Geophys. Res.*, *109*, B12310, doi:10.1029/2004JB003031.

Tregoning, P., et al. (1998), Estimation of current plate motions in Papua New Guinea from Global Positioning System observations, *J. Geophys. Res.*, *103*, 12,181–112,203.

Tregoning, P., M. Sambridge, H. McQueen, S. Toulmin, and T. Nicholson (2005), Tectonic interpretation of aftershock relocations in eastern Papua New Guinea using teleseismic data and the arrival pattern method, *Geophys. J. Int.*, *160*, 1103–1111.

Tsutsumi, H., R. S. Yeats, and G. J. Huftile (2001), Late Cenozoic tectonics of the northern Los Angeles fault system, California, *Geol. Soc. Am. Bull.*, *113*, 454–468.

Ward, S. N. (1982), On tsunami nucleation II. An instantaneous modulated line source, *Phys. Earth Planet. Inter.*, *27*, 273–285.

Wessel, P., and W. H. F. Smith (1995), New version of the Generic Mapping Tools released, *Eos Trans. AGU*, *76*(46), Fall Meet. Suppl., F329.

Yagi, Y., and M. Kikuchi (2000), Preliminary results of rupture process for November 16, 2000 New Ireland Region, Papua New Guinea earthquake, Earthquake Res. Inst., Univ. of Tokyo, Tokyo.

Yalciner, A. C., B. Alpar, Y. Altinok, O. Ilknur, and F. Imamura (2002), Tsunamis in the Sea of Marmara: Historical documents for the past, models for the future, *Mar. Geol.*, *190*, 445–463.